

See discussions, stats, and author profiles for this publication at: <https://www.researchgate.net/publication/258512069>

Dinitrogen Release from Arylpentazole: A Picosecond Time-Resolved Infrared, Spectroelectrochemical, and DFT Computational Study

ARTICLE *in* THE JOURNAL OF PHYSICAL CHEMISTRY A · NOVEMBER 2013

Impact Factor: 2.69 · DOI: 10.1021/jp4077454 · Source: PubMed

CITATIONS

8

READS

53

7 AUTHORS, INCLUDING:



Peter Portius

The University of Sheffield

44 PUBLICATIONS 822 CITATIONS

[SEE PROFILE](#)



František Hartl

University of Reading

165 PUBLICATIONS 3,383 CITATIONS

[SEE PROFILE](#)



Qiang Zeng

South China University of Technology

24 PUBLICATIONS 125 CITATIONS

[SEE PROFILE](#)



Anthony J. H. M. Meijer

The University of Sheffield

97 PUBLICATIONS 1,506 CITATIONS

[SEE PROFILE](#)

Dinitrogen Release from Arylpentazole: A Picosecond Time-Resolved Infrared, Spectroelectrochemical, and DFT Computational Study

Peter Portius,^{*,†} Martin Davis,[†] Rory Campbell,[†] František Hartl,^{*,§} Qiang Zeng,[§] Anthony J. H. M. Meijer,[†] and Michael Towrie[†]

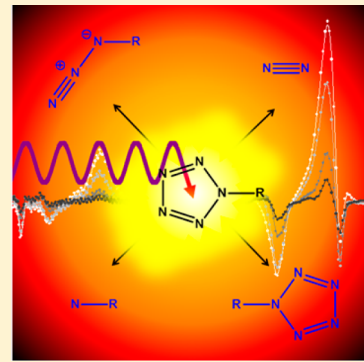
[†]Department of Chemistry, University of Sheffield, Brook Hill, Sheffield, S3 7HF United Kingdom

[‡]Central Laser Facility, STFC Rutherford Appleton Laboratory, Harwell Science and Innovation Campus, Didcot, OX11 0QX United Kingdom

[§]Department of Chemistry, University of Reading, Whiteknights, Reading, RG6 6AD United Kingdom

Supporting Information

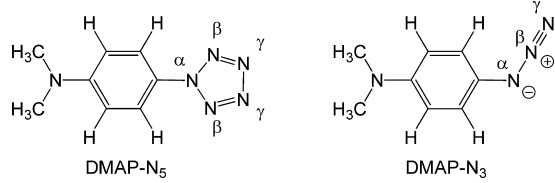
ABSTRACT: *p*-(Dimethylamino)phenyl pentazole, DMAP-N₅ (DMAP = Me₂N-C₆H₄), was characterized by picosecond transient infrared spectroscopy and infrared spectroelectrochemistry. Femtosecond laser excitation at 310 or 330 nm produces the DMAP-N₅ (S_1) excited state, part of which returns to the ground state ($\tau = 82 \pm 4$ ps), while DMAP-N and DMAP-N₃ (S_0) are generated as double and single N₂-loss photoproducts with $\eta \approx 0.14$. The lifetime of DMAP-N₅ (S_1) is temperature and solvent dependent. [DMAP-N₃]⁺ is produced from DMAP-N₅ in a quasireversible, one-electron oxidation process ($E_{1/2} = +0.67$ V). Control experiments with DMAP-N₃ support the findings. DFT B3LYP/6-311G** calculations were used to identify DMAP-N₅ (S_1), DMAP-N₃⁺, and DMAP-N in the infrared spectra. Both DMAP-N₅ (S_1) and [DMAP-N₅]⁺ have a weakened N₅ ring structure.



INTRODUCTION

Nitrogen-rich molecules have a major advantage over conventional solutions to the problem of chemical energy storage, since their decomposition releases almost exclusively the environmentally friendly dinitrogen.¹ In the search for stable nitrogen-rich compounds the synthetically most important approaches have been the coordination of azide anions (N₃⁻)^{2–5} and the derivatization of tetrazole (R-CN₄-R')^{1,6–8} which are the basis of applications in pyrotechnics and primary explosives.^{9–11} However, extremely nitrogen-rich systems are likely to require novel, homonuclear polynitrogen species larger than N₃. The synthesis of such species, albeit challenging, has been accomplished for N₅⁺¹² whereas only analytical or indirect evidence exists for N₄^{13,14} and the pentazolate anion, N₅⁻^{15–18,23,25} traces of which were produced and detected by laser desorption ionization ($\lambda = 337$ nm) of *p*-Me₂N-C₆H₄-N₅ (DMAP-N₅, Chart 1), mass spectrometry,¹⁷ and combined ESI-MS-MS experiments.¹⁸

Chart 1. *p*-(Dimethylamino)phenyl Pentazole (DMAP-N₅) and *p*-(Dimethylamino)phenyl Azide (DMAP-N₃)



Cyclo-N₅⁻ is particularly interesting as it may act as a 2e or 6e donor ligand analogous to η^1 ^{19,20} or η^2 -bound^{20,21} N₃⁻ and cyclopentadienide,^{20,22–24} respectively. Attempts at the bulk synthesis of N₅⁻ such as N-dearylation of aryl-N₅ pentazole by ceric ammonium nitrate have failed thus far. The role that pentazoles play as potential precursors in the yet undiscovered synthetic method for pentazolate anions²⁵ provides motivation for a detailed investigation of their excited state and redox chemistry. As unsaturated all-nitrogen heterocycles, all known pentazoles R-C₆H₄-N₅²⁶ (R = alkyl, Br, Cl, CF₃, CN, COOH, H,²⁷ NMe₂,²⁸ NO₂, O⁻,²⁹ OH, OEt, OMe, S⁻, and SO₃⁻³⁰) are thermolabile and decompose at ambient temperature to N₂ and R-C₆H₄-N₃.³¹ The decomposition rates decrease with increasing σ electron-withdrawing and π donating capabilities of the substituent R. DMAP-N₅ (Chart 1) is one of the most stable pentazoles, which forms upon reaction of a diazonium salt with NaN₃³² and does not decompose for many hours at 243 K in solution ($\tau \approx 2$ h, MeOH, 273 K).³³ Its crystal structure has been determined²⁸ and NMR spectra recorded.^{31,34} Ab initio calculations³⁵ revealed that the transition state for the elimination of N₂ is ca. 21 kcal mol⁻¹ (ΔG_{sol}^*) above the ground state and connects the ground state with the N₂-loss product by the concerted elongation of N_α-N_β and N_γ-N_γ bonds.

Received: August 2, 2013

Revised: November 4, 2013

Published: November 13, 2013

Whereas the unusual pentazoles have not been characterized photochemically, organic azides have been studied intensely and feature the loss of N_2 and the intermediary formation of nitrenes with high quantum yields on ultrafast time scales.^{36–38} Specifically, in a low temperature matrix, irradiation of DMAP-N₃^{39,40} (the azide directly related to DMAP-N₅) yields a triplet nitrene,⁴¹ which has also been detected in picosecond and nanosecond laser photolysis experiments by means of the DMAP-N (T_1) \leftarrow DMAP-N (T_0) absorption at 470 nm.⁴² In cyclohexane, DMAP-N (T_0) generates the azo compound DMAP-N=N-DMAP.⁴³ Calculations show that the DMAP-N (T_0) ground state lies >12 kcal mol⁻¹ below the lowest singlet state.⁴⁴

Only scarce reports are available on the cathodic electrochemistry (cyclic voltammetry) of substituted phenyl pentazoles and phenyl azides. For *p*-MeO-C₆H₄-N₅ irreversible reduction has been reported in MeCN ca. -2.4 V at 253 K.^{45,46} No spectral data are available for reduced or oxidized species. It was speculated that using transition metal salts as electrolytes, reduction induces cleavage of the aryl-N₅ bond and produces *cyclo*-N₅⁻ and the aryl radical, which ultimately leads to the production of hydroquinone.⁴⁵

This paper describes results of an investigation into the electronically excited state, redox chemistry, and the possibility of cleaving the aryl pentazole bond in *p*-(dimethylamino)-phenyl pentazole using a combination of ultrafast time-resolved infrared spectroscopy, infrared spectroelectrochemistry, and density functional theory.

RESULTS AND DISCUSSION

DMAP-N₅ Excited State and Reactivity. Picosecond time-resolved infrared absorbance spectra (ps-TRIR spectra) in the 1 ps to 1 ns time domain of *p*-(dimethylamino)phenyl pentazole (DMAP-N₅, Chart 1) in CH₂Cl₂ were recorded at 233 K under 310 nm, femtosecond excitation in the 1250 – 2200 cm⁻¹ spectral range (see Figures 1–3 in which the spectra are represented by plotting absorbance change (ΔA) vs. wavenumber (\bar{v})). In this range the FTIR spectra of the ground state exhibit absorption bands at 1608, 1533, 1384, 1448, 1485, 1518, 1524, 1365, and 1360 cm⁻¹, which could be assigned tentatively with the help of DFT calculations (see the Experimental Section and the SI). These ground state bands are fully bleached at 4 ps after the laser flash, while broad transient bands appear at 1304, 1376, 1477, 1490, and 1598 cm⁻¹ (Figure 1). The transient bands decay within the subsequent 200 ps while the bleached parent bands recover only partially. A set of weaker bands at 1375, 1440, 1505, and 1590 cm⁻¹ persist over the recorded time scale. In addition, initially broad transient bands rise in the region of the asymmetric azide stretches, $\nu(N_3)_{as}$, which are, however, much weaker ($\Delta A < 2 \times 10^{-4}$) than the parent bleaches. Within 30 ps after excitation these bands narrow and shift to higher wavenumbers at 2094 and 2125 cm⁻¹ (Figure 3). The latter transient bands are assigned to the DMAP-N₃ ground electronic state through a comparison with the FTIR spectrum of a genuine sample of DMAP-N₃ (vide infra and Figures S2 and S3). DMAP-N₃ absorbs in the region of the $\nu_{as}(N_3)$ stretching vibrations and exhibits two bands as a result of Fermi resonance.⁴⁷ Fermi resonance was observed in related aryl azides previously (Table 2 caption).^{48–50}

The rise of both $\nu(N_3)_{as}$ bands is synchronous and biexponential, which is attributed to the cooling of the vibrationally hot [DMAP-N₃][‡] ($\tau = 18 \pm 5$ ps), whereas the

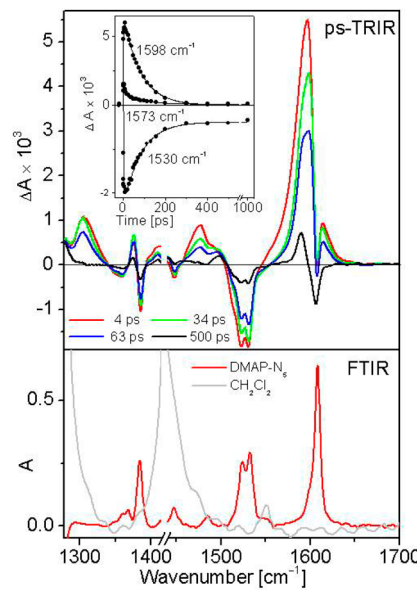


Figure 1. ps-TRIR spectra in CH₂Cl₂ at 233 K recorded at 4, 34, 63, and 500 ps after the fs excitation ($\lambda_{ex} = 310$ nm) (top); kinetic traces showing the cooling (1573 cm^{-1}) and decay of the electronically excited DMAP-N₅ (S_1) state (1598 cm^{-1}) and the partial ground state recovery of DMAP-N₅ (1530 cm^{-1}) (inset), and the FTIR spectrum (red line) of the ground state (bottom). The spectral ranges below 1275 and 1410–1440 cm⁻¹ are affected by CH₂Cl₂ absorptions (gray line).

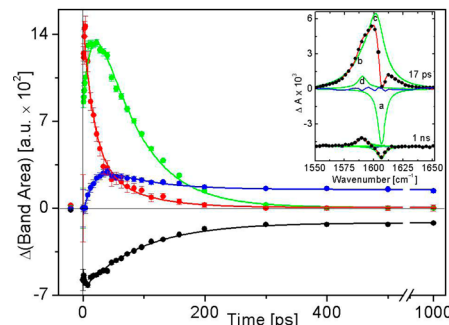


Figure 2. Picosecond kinetics in CH₂Cl₂ at 233 K derived from band area changes centered at 1606 (black dot, a), 1602 (green dot, c), 1592 (red dot, b), and 1590 cm⁻¹ (blue dot, d). Inset: spectra at 17 ps and 1 ns (see Figure 1) showing the individual absorption profiles (green), residual (blue) and fit curves (red) to the spectral data points (•).

slow component ($\tau = 106 \pm 25$ ps) indicates that much of DMAP-N₃ in the electronic ground state is produced from a slowly decaying precursor. Even though 500 ps after excitation the $\nu_{as}(N_3)$ transients of DMAP-N₃ have fully grown ($\Delta A_{max} \approx 2 \times 10^{-4}$), they are still considerably weaker than the prominent transient bands in the fingerprint region ($\Delta A \approx 7 \times 10^{-4}$). In combination with the absence of discernible bands of DMAP-N₃ in this spectral region (see FTIR spectrum of DMAP-N₃, Figure S3) it is suggested that DMAP-N₃ is a minor photoproduct under the 310 nm excitation regime in CH₂Cl₂. The most striking feature in the early ps-TRIR spectra is the very intense and initially broad transient absorption at 1590–1602 cm⁻¹ belonging to a combined symmetric C₆ ring vibration and CN stretching, which decays during the parent recovery process. Band shape analysis of this absorption reveals

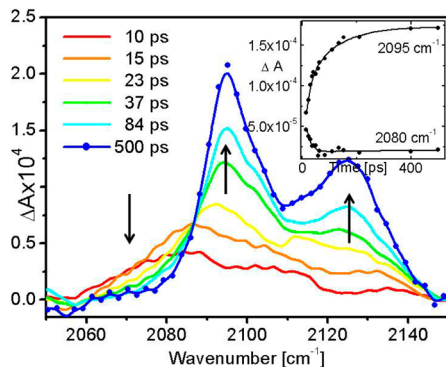


Figure 3. ps-TRIR spectra of DMAP-N₃ (CH_2Cl_2 , 233 K), recorded in the $\nu(\text{N}_3)_{\text{as}}$ stretch region after the fs excitation ($\lambda_{\text{ex}} = 310 \text{ nm}$). Inset: kinetic traces of the rise of DMAP-N₃ (S_0) at 2095 cm^{-1} , and of the vibrational cooling at 2080 cm^{-1} , $\tau = 106 \pm 25$ and $18 \pm 5 \text{ ps}$, respectively.

overlapping components (Figure 2, inset) centered at 1590 (d) and 1602 cm^{-1} (c).

While the component c is strong and short-lived, the component d is weak and noticeable only from 17 ps onward. Additional, broad absorption bands tail the main band at the low energy side. Using Voigt profiles for the transient (c and d) and parent bleach bands (a, 1606 cm^{-1}) and for the very short-lived, broad absorption centered at 1592 cm^{-1} (b), results in a good fit of the spectral data points throughout the entire time domain. Kinetic plots (Figure 2) show rapid decay of b and rise of c with lifetimes of $\tau = 12(\pm 1)$ and $10(\pm 1) \text{ ps}$, respectively. The transient b, identified by the broad absorption at 1592 cm^{-1} , most likely involves population of vibrationally hot states from which it decays to form c. This assignment is in agreement with the synchronous rise of c and the relative position of b with respect to c at lower wavenumber. Transient c decays itself on a longer time scale ($\tau = 82(\pm 4) \text{ ps}$), while the parent band (a) recovers ($\tau = 96(\pm 5) \text{ ps}$, Table 1). The bleached parent

Table 1. Lifetimes^a of Species Generated upon Femtosecond Excitation ($\lambda_{\text{ex}} = 310 \text{ nm}$) of DMAP-N₃ at 233 K in CH_2Cl_2 , DMAP = *p*-Me₂N-C₆H₄

species	recovery	rise	decay	$\nu [\text{cm}^{-1}]^c$
DMAP-N ₃ (S_0)	96 ± 5			1606 (a)
DMAP-N ₃ ^d (S_1)			12 ± 5	1592 (b)
DMAP-N ₃ (S_1)	10 ± 5		82 ± 4	1602 (c)
DMAP-N ₃ ^d (S_0)			18 ± 5	
DMAP-N ₃ (S_0)	106 ± 25			
DMAP-N ^d		8 ± 1^b		
DMAP-N	17 ± 3^b	e		1590 (d)

^a τ (estimated standard error) [ps]. ^b CH_2Cl_2 solution of DMAP-N₃.

^cThe labels a, b, c, and d denote characteristic transient bands shown in Figure 2. ^dHot state. ^eNo decay during the time scale of the experiment.

band at 1530 cm^{-1} is unaffected by overlap and was found to recover with a similar lifetime of $83(\pm 5) \text{ ps}$. The ground state of DMAP-N₃ is recovered on the ps time-scale by 86%.

In a control experiment, the related azide DMAP-N₃ (vide supra) was investigated under identical conditions (Figure 4). The ps-TRIR spectra of DMAP-N₃ show bleaching of the parent bands at $1601, 1513, 1481, 1445, 1354$, and 1291 cm^{-1} , which, however, do not recover. Intriguingly, the transient

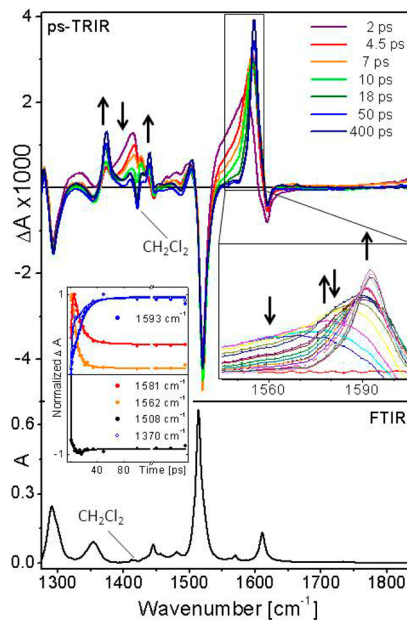


Figure 4. ps-TRIR spectra of DMAP-N₃ in CH_2Cl_2 recorded at 233 K ($\lambda_{\text{ex}} = 310 \text{ nm}$) (top); FTIR of the ground state (bottom). Left inset: kinetics of parent bleach (1518 cm^{-1}), vibrational cooling (1562 cm^{-1} , ↓), decay of transient (1581 cm^{-1} , ↑↓), and growth of vibrationally cold photoproduct (1593 cm^{-1} , ↑).

bands below 2000 cm^{-1} ($1590, 1505, 1440$, and 1375 cm^{-1}) persist on the ps time scale and match those found in the ps-TRIR spectra of DMAP-N₃, suggesting therefore that the latter bands belong to the same photoproduct.

In the absence of other, intense transient absorptions, the evolution of the dominant transient at 1590 cm^{-1} (band d) could be analyzed (Figure 4, insets) showing again broad bands at the low-energy side of the main transient, which are assigned to a vibrationally hot species. Cooling of the latter appears to produce a new transient at ca. 1581 cm^{-1} , the decay of which gives rise to the band of the permanent photoproduct (b and d). Again, the transient absorption band assigned to a combined symmetric C₆ ring vibration and CN stretching vibration associated with the bleached parent band is much more intense than the corresponding bleached parent band. As in the ps-TRIR spectra of the pentazole in this region, vibrational cooling can be observed with a slightly shorter lifetime ($\tau = 8.3(\pm 0.6) \text{ ps}$, see Figure 4, inset).

It is clear that the permanent transient bands in the TRIR spectra of DMAP-N₃ cannot arise from a photoreaction involving the azide DMAP-N₃ which is potentially present as a result of thermal decomposition of the pentazole and which also absorbs at 310 nm, since a corresponding intense bleach at 1514 cm^{-1} (Table 1) is absent from the spectra, due to the lack of bleached absorption bands of the DMAP-N₃ groundstate in the TRIR spectra of DMAP-N₃.

Using DFT (vide infra), vibrational frequency calculations were performed for the electronic ground state and the lowest singlet excited state of both pentazole (DMAP-N₃) as well as for the azide (DMAP-N₃) and the nitrenes DMAP-N (T_0) and (S_1). Predicted frequencies and intensities of the prominent transient bands strongly indicate that the lowest lying electronic excited state is a singlet, DMAP-N₃ (S_1), and gives rise to the absorption band c as the major transient species.

The bands at 1304, 1376, and 1477 cm^{-1} have the same lifetime as c and belong to this species. DFT was employed to evaluate the trends in the energy of fundamental vibrations^{51,52} across species (vide infra). These calculations predict a strong band at a slightly lower energy (1574 cm^{-1}) compared to the related ground state bleach (1596 cm^{-1}) and this is indeed observed ($1602 \text{ vs. } 1606 \text{ cm}^{-1}$). On the other hand, for the lowest triplet excited state, the same fundamental vibration is predicted at a higher energy (for assignments of observed and calculated vibrational frequencies see the SI). DMAP-N₅ (S₁) is formed vibrationally hot, giving rise to band narrowing and a fast decay component of $15(\pm 4)$ ps that can be observed at 1602 cm^{-1} at the low energy side of the main transient band. In order to investigate whether the decay of the excited state is an activated process, the temperature dependence of the DMAP-N₅ (S₁) decay rate was checked by an Arrhenius plot between 232 and 273 K (Figure 5). In CD₃CN solution, the activation

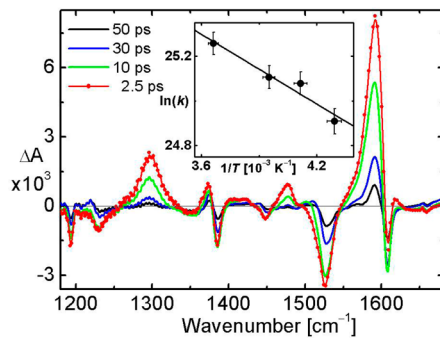


Figure 5. ps-TRIR spectra of DMAP-N₅ at ca. 233 K in CD₃CN recorded after fs excitation ($\lambda_{\text{ex}} = 330 \text{ nm}$). Inset: temperature dependence of parent recovery (273 to 233 K).

energy (E_a) and preexponential factor (A) were found to be $4.3(\pm 0.7) \text{ kJ mol}^{-1}$ and $6(\pm 2) \times 10^{11}$, respectively, which indicate that a barrier exists on the pathway of the DMAP-N₅ (S₁) decay.

As can be deduced from the TRIR spectrum recorded 500 ps after the laser flash (Figure 1, black line) and from the kinetic trace of the parent bleach at 1608 cm^{-1} , a minor part of photoexcited DMAP-N₅ forms a long-lived photoproduct. Correspondingly, weak, residual transient bands and parent bleaches are persistent even at 1000 ps. The spectral positions of the observed persistent transient bands at 1590, 1505, 1440, and 1375 cm^{-1} (Figure 4) agree best with those predicted for vibrations with high oscillator strength of DMAP-N (T₀), while the fast decaying bands 1580, 1480, 1465, 1412, and 1333 are assigned tentatively to DMAP-N (S₁) (see SI, Table S2).

ps-TRIR spectra of DMAP-N₅ were recorded in complementing spectral windows free of solvent absorptions in CH₂Cl₂ (Figure 1), CD₃CN (Figure 5), CD₃OD, and THF (SI) using 330 nm excitation. The transient bands of DMAP-N₅ (S₁) feature in all of these solvents. While excitation at 330 nm does not significantly change the ps-TRIR spectra compared to 310 nm, the DMAP-N₅ (S₁) lifetime changes (CH₂Cl₂, $76(\pm 11)$ ps at ~ 234 K; CD₃CN, $22(\pm 8)$ ps at ~ 233 K; CD₃OD, $32(\pm 4)$ ps at ~ 238 K; THF, $8(\pm 1)$ ps at ~ 238 K). Throughout, parent recovery was found at or above 80%, with a significant difference between solutions in CH₂Cl₂ and CD₃OD ($86(\pm 3)\%$ and $97(\pm 3)\%$).

Cyclic Voltammetry and Anodic IR Spectroelectrochemistry of DMAP-N₃.

The spectroelectrochemistry of

DMAP-N₅ and DMAP-N₃ was investigated not only in order to test the possibility of cleaving the aryl pentazole bond and assess the stability of the reduced and oxidized Ar–N₅, but also to assist the assignment of the intermediates of the photo-reaction discussed above. The cyclic voltammogram of DMAP-N₃ in CH₂Cl₂/("Bu₄N)PF₆ (TBAH) shows a one-electron anodic wave at $E_{1/2} = +0.32 \text{ V}$ vs. Fc/Fc⁺ while no electrochemical reduction is observed within the potential window of the solvent/electrolyte combination. The oxidation of DMAP-N₃ to the corresponding radical cation is fully reversible at 243 K, the peak current ratio $i_c/i_a = 1$ at $v \geq 100 \text{ mV s}^{-1}$ and the peak-to-peak potential separation $\Delta E_p = 100 \text{ mV}$ being identical with the value recorded for the reduction of the internal cobaltocenium standard, [CoCp₂]PF₆.

Further lowering the temperature slows down the electron transfer kinetics significantly and raises the ΔE_p value up to 320 mV at 195 K. At ambient temperature, the oxidation of DMAP-N₃ triggers a secondary reaction, as indicated by $i_c/i_a < 1$ (0.55 at 293 K) and the appearance of new cathodic wave at $E_{p,c} = -0.13 \text{ V}$ vs. FeCp₂/FeCp₂⁺ (Fc/Fc⁺) on the reverse potential scan, which belongs to an unassigned oxidation product that was characterized in situ by IR spectroscopy (vide infra). IR spectral monitoring of the one-electron oxidation product of DMAP-N₃ was conducted in CH₂Cl₂/TBAH within a low-temperature OTTLE cell at 226 and 241 K. At both temperatures the electrogenerated cation [DMAP-N₃]⁺ was completely stable. The oxidation of DMAP-N₃ was accompanied by the disappearance of absorption bands at 2128(m), 2096(s), 2017(vw), 1613(w), 1514(s), 1363(vw), 1291(w), 1225(vw), 1171(vw), and 1131(vw) cm^{-1} (Figure 6). The cationic product was found to absorb at 2413(vw), 2217(w), 2146(w), 2124(m), 2106(vs), 1930(vw), 1590(m), 1323(m), 1302(s), and 1198(w) cm^{-1} (see Figure 6 and Tables 2 and S3). Back-reduction of [DMAP-N₃]⁺ led to nearly complete (90%) regeneration of the neutral parent compound. Rapid potential-step oxidation of DMAP-N₃ at 273 K formed first the corresponding cation which slowly transformed to a single secondary product absorbing in the $\nu_{as}(N_3)$ stretching region at 2140(m-w), 2128(sh), and 2115(m) cm^{-1} (see Figure 7).

Cyclic Voltammetry and Anodic IR Spectroelectrochemistry of DMAP-N₅. In contrast to DMAP-N₃, the cyclic voltammogram of DMAP-N₅ in CH₂Cl₂/TBAH exhibits waves both in the cathodic and anodic regions. The electrolyte solution temperature was kept at 243 K in order to avoid the thermal decomposition of the pentazole. The cathodic wave at $E_{p,c} = -2.68 \text{ V}$ vs. Fc/Fc⁺ corresponds to a completely irreversible two-electron reduction *via* the electron transfer, chemical reaction, electron transfer (ECE) mechanism, in agreement with the dissociation of the reduced pentazolyl moiety from the para-substituted phenyl ring proposed in the literature for the *p*-MeO-C₆H₄-N₅ derivative. On the other hand, the oxidation of DMAP-N₅ at $E_{1/2} = +0.67 \text{ V}$ vs. Fc/Fc⁺ is an irreversible one-electron process ($\Delta E_p = 165 \text{ mV}$, $i_c/i_a = 0.65$, at $v = 100 \text{ mV s}^{-1}$). The ultimate product is the oxidized azido compound, [DMAP-N₃]⁺, as revealed unambiguously by IR monitoring (vide infra). In the cyclic voltammetry cell, the detection of [DMAP-N₃]⁺ on the reverse cathodic scan was complicated by the partial thermal decomposition of the pentazole to azide in the bulk solution.

An IR spectroelectrochemical experiment with DMAP-N₅ was carried out at 248 K in CH₂Cl₂/TBAH saturated with argon. The stock electrolyte solution of ca. $1 \times 10^{-3} \text{ M}$ DMAP-N₅ was prepared in a Schlenk tube at 238 K and cannula-

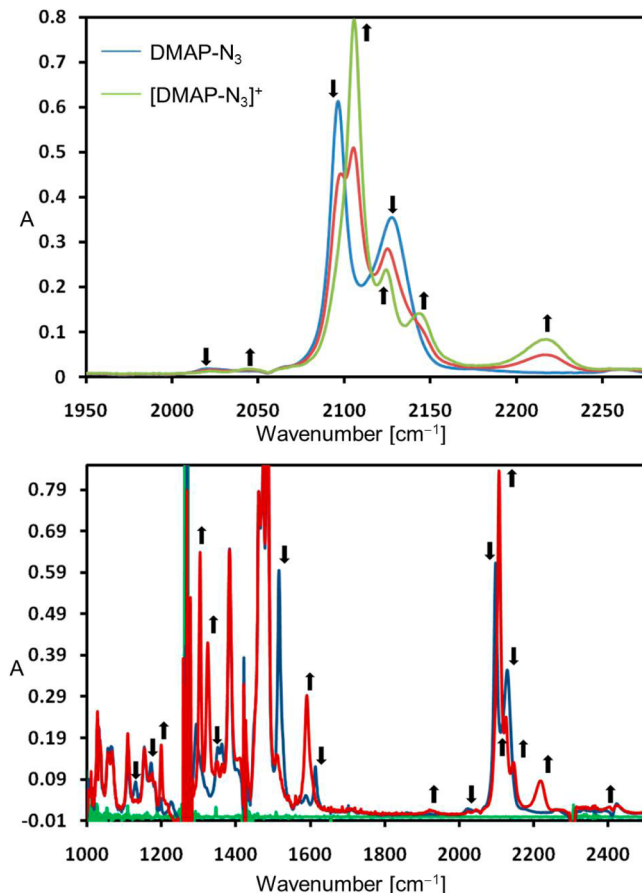


Figure 6. FTIR spectra showing the spectral changes caused by the one-electron oxidation of DMAP-N₃ in CH₂Cl₂/TBAH at 241 K within the OTTLE cell. Top: $\nu(\text{N}_3)_{\text{as}}$ region, before (blue line), during (red line), and after (green line). Bottom: 1000–2500 cm⁻¹ region, DMAP-N₃ (blue line), [DMAP-N₃]⁺ (red line), and baseline (green line). IR absorbance changes are indicated ($\downarrow\uparrow$).

Table 2. Spectral Positions [cm⁻¹] of Prominent IR Absorption Bands of DMAP-N₃ and [DMAP-N₃]⁺ in CH₂Cl₂

vibration	DMAP-N ₃		[DMAP-N ₃] ⁺	
	obsd. ^b	calcd. ^c	obsd. ^b	calcd. ^c
$\nu(\text{N}_3)_{\text{as}}^d$	2128(m) 2096(s)	2221(1708) 2124(m) 2106(vs)	2146(w) 2124(m)	2239(1713) 1639(310)
sym. ring ^e	1613(w)	1651(133)	1590(m)	1639(310)
as. ring ^e	1514(s) 1363(vw)	1546(517) 1381(106)	1512(w)	1541(151)
$\nu(\text{N}_3)_s$	1291(w)	1360(343)	1323(m)	1379(722) 1302(s)
				1334(119)

^aDMAP = *p*-Me₂N-C₆H₄. ^bVery weak (vw), weak (w), medium (m), strong (s), and very strong (vs). ^cDFT, B3LYP/6-311G** calculations, intensities [km mol⁻¹] in parentheses (see Table S3). ^d $\nu(\text{N}_3)_{\text{s(as)}}$ symmetric (asymmetric) azide stretch, $\nu(\text{N}_3)_{\text{as}}$ band splitting due to Fermi resonance with the $\nu(\text{N}_3)_s + \delta(\text{N}_3)$ combination (1291 cm⁻¹ + 813 cm⁻¹ = 2104 cm⁻¹), compare to ref 50. ^eSymmetric (asymmetric) ring vibration —CN stretch.

transferred promptly under argon into the precooled low-temperature OTTLE cell. The FTIR spectra revealed only the presence of DMAP-N₅ absorbing at 1609(vs), 1533(m), 1525(m), 1490(w), and 1386(m) cm⁻¹ that remained stable

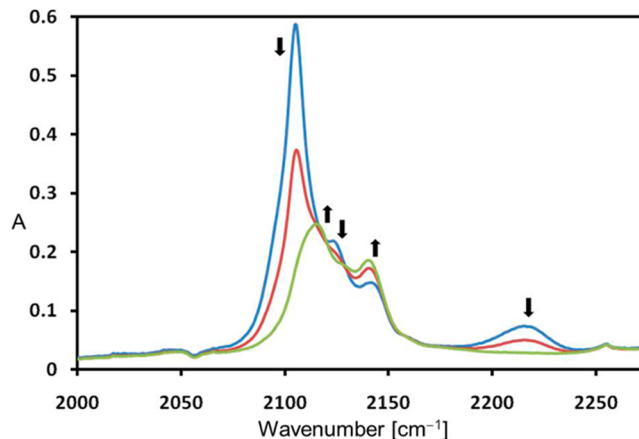


Figure 7. FTIR spectra recorded before (blue line), during (red line), and after (green line) the thermal conversion of [DMAP-N₃]⁺ in CH₂Cl₂/TBAH at 273 K.

at 248 K. In situ oxidation of the parent pentazole resulted in ca. 60% conversion to a product absorbing at 2217, 2142, 2112(sh), 2105, 1590, 1322, and 1302 cm⁻¹ (Figure 8). The

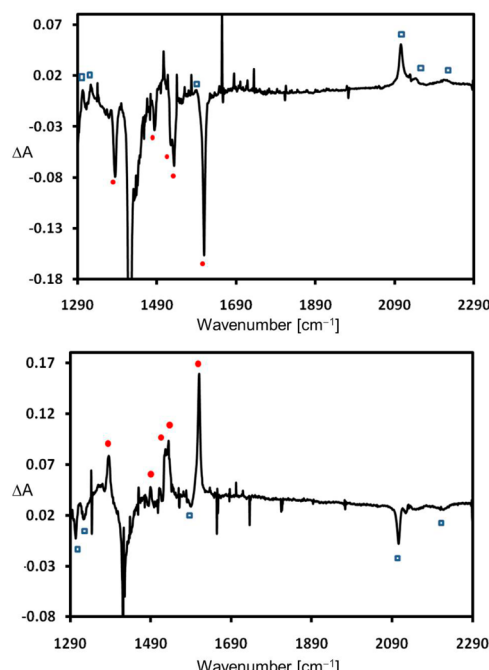


Figure 8. FTIR absorbance difference spectra showing the anodic conversion of DMAP-N₅ (red dot) to [DMAP-N₃]⁺ (blue square) in CH₂Cl₂/TBAH at 243 K within the low-temperature OTTLE cell (top), and recovery of DMAP-N₅ upon back reduction of [DMAP-N₃]⁺ in the thin-solution layer of the cell (bottom). Nonlabeled bands are due to the electrolyte, solvent, or moisture in the optical path.

spectral positions of the peak maxima of this product are characteristic of the cationic azide [DMAP-N₃]⁺ observed earlier (cf. Figure 7 and Table 2). Surprisingly, the elimination of N₂ from the primary anodic product [DMAP-N₅]⁺ is consistent with a reversible mechanism at the Pt-minigrid working electrode in the viscous, thin solution layer of the OTTLE cell; for a reverse, rapid, cathodic potential step led to ca. 80% recovery of parent DMAP-N₅ whereas no DMAP-N₃ was observed (Figure 8). Any diffusion of nonoxidized DMAP-

N_5 in the chilled thin solution layer can be excluded. Further investigations are underway to provide an explanation for this remarkable redox behavior. The reduction of DMAP- N_5 at -2.68 V was irreversible and could not be monitored by IR spectroscopy using the OTTLE cell setup due to passivation of the working electrode.

DFT Calculations. The minimum energy geometry of DMAP- N_5 was determined by density functional theory (DFT) calculations at the B3LYP/6-311G** level (see the Experimental Section, relative energies are reported in the SI). The minimum structure of the ground state (S_0) compares very well with the planar molecular structure found in the crystal²⁸ (Figure 9a). The first excited state, [DMAP- N_5] (S_1), however,

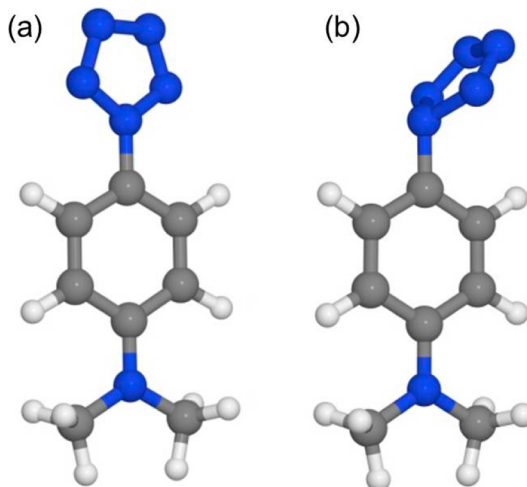


Figure 9. Ball-and-stick diagrams of electronic ground (S_0) (a) and excited states (S_1) (b) of DMAP- N_5 ; C, gray; H, white; N, blue.

features a twisted phenyl pentazole structure with a pyramidalized N_α atom (Figure 9b). As a consequence, N_α – N_β bonds at 1.44 Å are lengthened, while both N_β – N_γ and N_γ – N_γ bonds at 1.32 and 1.31 Å are largely unchanged in comparison with the ground state (1.32 , 1.30 , and 1.33 Å, respectively). The N_α – N_β elongation suggests a considerable weakening of this bond compared to the other N–N bonds.

An electronic absorption spectrum of DMAP- N_5 was calculated using time dependent DFT (TDDFT) based on the ground state geometry. These calculations indicate that the lowest excited singlet state at 353 nm is the only state accessible with the excitation wavelength used in the TRIR experiments ($\lambda_{\text{exc}} = 310$ and 330 nm), since other electronic transitions at this wavelength have low oscillator strengths (Figures S10 and S11). The nature of this transition is an internal (DMAP group)-to-(N_5 ring) charge transfer, which can be gleaned from the electron density difference plot in Figure 10 and shows analogies with that of DMAP-CN.⁵³ Intriguingly, the electron density does not increase evenly across the pentazolyl moiety but increases less at the N_α – N_β bonds than elsewhere on the N_5 ring. This suggests that the N_α – N_β bonds will be weakened in the excited state, as it is clear from the optimization of the S_1 state. Hence, the excitation at 310 or 330 nm in the ps-TRIR experiments populates the first excited singlet state with an excess energy dumped into excited vibrational levels and this prepares the N–N bond cleavage.

The scaled vibrational frequencies and oscillator strengths of ground state and first excited state (Figure 11) show adequate

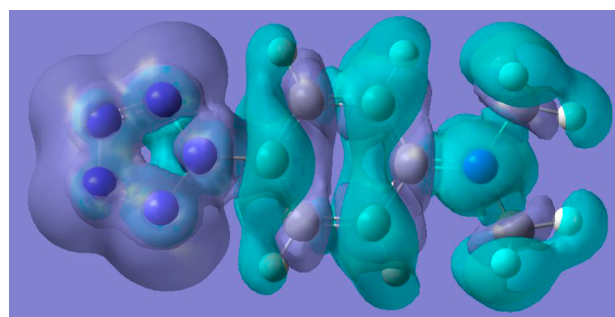


Figure 10. Electron density difference plot between ground (S_0) and excited (S_1) states at the S_0 geometry of DMAP- N_5 . The turquoise and light blue colors indicate a decrease or increase, respectively, in the electron density in S_1 compared to S_0 within the envelopes; ball-and-stick diagram: C, gray; H, white; N, blue.

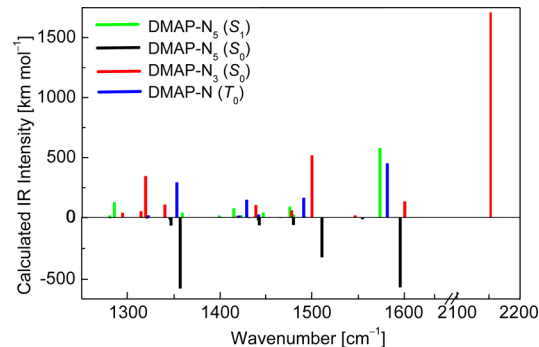


Figure 11. Stick spectra of calculated scaled vibrational frequencies vs. IR intensity of DMAP- N_5 (S_1), DMAP- N_5 (S_0), and DMAP- N (T_0) (up) and DMAP- N_5 (S_0) (down), at the B3LYP/6-311G** level using the polarizable continuum model with parameters for CH_2Cl_2 .

similarity with the values observed in the experiment for the ground state bleach bands and the transient bands present at 10 to 200 ps in the TRIR spectra (see Figure 1). It can therefore be assumed that the nature of the transient species has been correctly identified.

The reaction initiated by the photoexcitation of DMAP- N_5 is most likely dominated by non-Born–Oppenheimer dynamics^{54,55} leading to dissociation as well as the population of the S_1 excited state of DMAP- N_5 . This excited state is formed vibrationally hot, and with a lifetime of several tens of picoseconds, decays primarily to the electronic ground state and to the immediate successor species on a time scale concurrent with vibrational relaxation. The detectable products are the nitrene, DMAP- N , and the azide DMAP- N_3 . Direct formation of nitrene from DMAP- N_5 would imply a simultaneous release of two N_2 molecules, which is unlikely. A plausible pathway involves the DMAP- N_5 (S_1) hot electronic excited state to produce one N_2 -molecule and a singlet excited state of the azide, DMAP- N_3^* . Exploratory DFT calculations (vide infra) have revealed that DMAP- N_3^* (S_1) has dissociative character which rationalizes results obtained from the ps TRIR experiments with DMAP- N_3 , according to which practically no recovery of the ground state was observed; hence, the photoexcitation of DMAP- N_3 is irreversible. Accordingly, this intermediate species would decay on the ultrafast time scale before it can equilibrate with the surrounding solvent, with the formation of vibrationally hot nitrene, which converts to its vibrationally relaxed triplet ground state DMAP- N (T_0) as long-lived photoproduct detected in the TRIR experiments

with both DMAP-N₃ and DMAP-N₅. The ultrafast, non-equilibrium character of the processes involved suggests multiple, ultrafast, potential energy surface crossings via a conical intersection, which indeed are typical for many organic photochemical reactions, such as the photodissociation of formaldehyde⁵⁶ and organic azides.⁵⁷ A detailed investigation of the reaction dynamics including the calculation of conical intersections within a multireference framework lies outside of the scope of this paper. Instead, a more approximate approach was chosen with the goal of obtaining a qualitative understanding of the experimental data. To achieve this goal, a single-reference standard DFT approach should be sufficient. Thus, the reactivity of the excited state was investigated theoretically by lengthening one N_α–N_β bond length to 1.91 Å and reoptimizing the molecule. On the ground state surface, the molecule returned to the ground state geometry. On the excited state surface, N₂ was released in a concerted fashion with N_α–N_β and N_γ–N_γ bonds breaking simultaneously as opposed to a prior uncurling of the N₅ ring. The calculation on the excited state surface was stopped after N₂ was released, which resulted in the structure shown in Figure 12a. The N–N distance in the N₂ fragment is 1.11 Å, which points to a dinitrogen molecule in the ground state associated to a DMAP-N₃ (S₁) fragment.

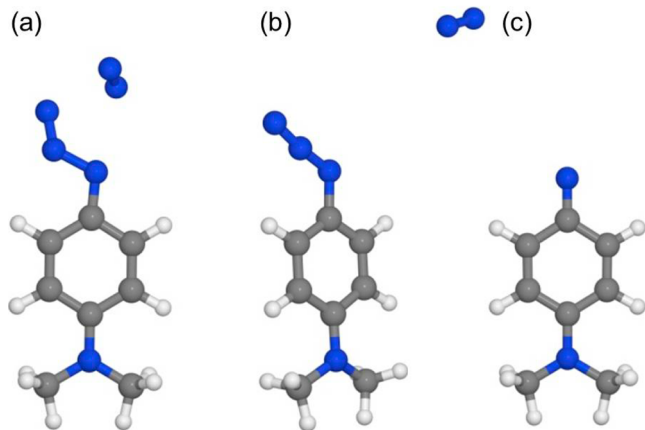


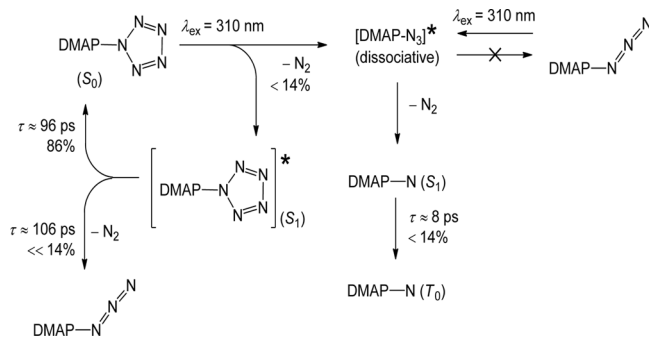
Figure 12. Ball-and-stick diagrams of the structures obtained from DMAP-N₅ with one N_α–N_β bond lengthened to 1.91 Å in the singlet excited state (a); from DMAP-N₃ in the electronic ground state (b) and from DMAP-N₃ in the singlet excited state (c); C, gray; H, white; N, blue.

In order to investigate the nature of DMAP-N₃ (S₁) fragment further, its coordinates were taken as the input in a geometry optimization of both the ground state and singlet excited state surfaces. While the optimization of the ground state surface resulted in a stable structure identical with DMAP-N₃ (S₀; Figure 12b), the optimization on the excited state surface was complicated by a second elimination of N₂ which lead to the nitrene DMAP-N (S₁; Figure 12c). Restricted optimizations were also performed with the N_α–N_β bond set to 1.37 and 1.47 Å, respectively, which returned structures 65.5 and 62.5 kJ mol⁻¹ higher in energy than the species shown in Figure 12c.

Thus, the ps TRIR spectra can be interpreted in terms of the electronic excited state DMAP-N₅* being formed upon 310 or 330 nm excitation with excess excitation energy converted into vibrational energy in DMAP-N₅* (S₁). DMAP-N₅* (S₁) is subject to vibrational cooling and forms DMAP-N₅ (S₁), which returns to the ground state DMAP-N₅ (S₀) and eliminates N₂.

This result removes the possibility of local minima other than the ones already identified and renders a stable DMAP-N₃ (S₁) unlikely. In order to exclude any possibility of N₂ release from the ground state surface of DMAP-N₅, the geometry with the N_α–N_β bond of 1.91 Å, described above, was also used for a transition state search on the ground state surface. A transition state was found with the pentazole ring perpendicular to the phenyl ring, as evidenced by the single imaginary frequency, similarly to the transition state found by Benin et al.²⁹ However, further inspection of this model shows that it is a transition state for the rotation of the entire N₅ ring relative to the phenyl ring, thus excluding any release of N₂ via this pathway. The N₂ loss product, DMAP-N₃, has an excited state structure, only a small part of which decays to the electronic ground state, DMAP-N₃ (S₀), while the majority extrudes a second dinitrogen molecule to produce the ultimate photoproduct on the ps time scale, DMAP-N (T₀; Scheme 1).

Scheme 1. Photoreactions of DMAP-N₅ and DMAP-N₃ in CH₂Cl₂ at 233 K



Intriguingly, the excited state DMAP-N₅ (S₁) has a much less dissociative nature than the azido analog DMAP-N₃ (S₁) and as much as 86% of the ground state DMAP-N₅ (S₀) are recovered compared to no ground state recovery after excitation of DMAP-N₃. The DFT calculations suggest rapid loss of N₂ on the singlet excited (S₁) surface which results in the formation of DMAP-N₃ (S₁), only a small part of which decays to DMAP-N₃ (S₀). Therefore, it has to be assumed that the system does not leave the singlet excited state surface, with DMAP-N₃ (S₁) being the transient state which leads directly to the formation of the singlet nitrene DMAP-N (S₁), as shown by the calculations. DMAP-N (S₁) can decay back to the singlet ground state or interconvert to DMAP-N (T₀) in the ground triplet state. This interpretation is supported by the ps-TRIR data obtained under identical conditions of both genuine DMAP-N₃ and DMAP-N₅ which form an identical photoproduct with different quantum yields. The absence of absorption bands in the 1800 to 1900 cm⁻¹ region (CN stretches) excludes the presence of dehydroazepine as an intramolecular nitrene insertion product on the picosecond time scale.⁵⁸ It should be noted here that the above picture is only qualitative. The precise mechanism and dynamics of the formation of DMAP-N from DMAP-N₅ via DMAP-N₃ is likely to be dominated by non-Born–Oppenheimer dynamics as indicated above and would require much more extensive calculations to resolve, which are outside of the scope of this paper.

DFT calculations have also been employed in order to investigate electronic and structural changes in DMAP-N₅ upon one-electron oxidation (see Table S3). The optimized structure

of $[\text{DMAP-N}_5]^+$ possesses a coplanar arrangement of phenyl and pentazole rings. Oxidation causes the elongation of $\text{N}_\alpha-\text{N}_\beta$ and $\text{N}_\gamma-\text{N}_\gamma$ (1.34 and 1.36 Å) and contraction of the $\text{N}_\beta-\text{N}_\gamma$ bonds (1.29 Å) in comparison with the neutral species, which again can be seen as a preparation of the release of N_2 . This change is caused by a reduction in σ electron density which is only partially counterbalanced by an increase in π electron density along the $\text{N}_\alpha-\text{N}_\beta$ and $\text{N}_\gamma-\text{N}_\gamma$ bonds (see Figure 13).

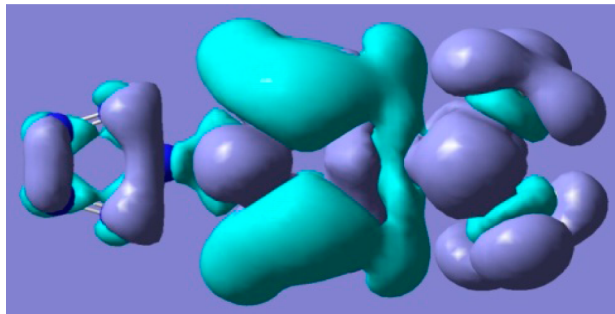


Figure 13. Electron density difference plot of $[\text{DMAP-N}_5]^+$ with turquoise envelopes indicating a decrease and light blue envelopes indicating an increase of the electron density relative to DMAP-N_5 .

CONCLUSIONS

The combination of experiment and theory presented in this study reveals the nature of a long-lived singlet excited state of *p*-(dimethylamino)phenyl pentazole (DMAP-N_5) which is accessible by 310 or 330 nm laser excitation. In the excited state, the N–N bonds of the pentazoly ring are weakened and lead to the release of dinitrogen. The quantum yield of N_2 photodissociation is much less effective than in the directly related *p*-(dimethylamino)phenyl azide (DMAP-N_3), with 86% of the excited sample being recovered to the electronic ground state.

Photolysis of DMAP-N_5 and DMAP-N_3 leads to the same photoproduct (Scheme 1) upon single or double N_2 -loss, respectively, with the former also producing DMAP-N_3 . Ab initio quantum chemical calculations in the ground and excited states show reduced electron density in the regions connecting the relevant nitrogen atoms in the pentazole ring. The cyclic voltammetric experiments revealed that the oxidation of DMAP-N_5 produces $[\text{DMAP-N}_3]^+$ which was verified independently by IR OTTLE measurements with the reversible oxidation of $[\text{DMAP-N}_3]$. The data on the one-electron oxidation of DMAP-N_5 leading to $[\text{DMAP-N}_3]^+$, which was obtained with the employed cell setup, is consistent with a reversible mechanism. Under the chosen conditions, neither photoexcitation nor electrochemical oxidation cleaves the aryl-pentazole bond of DMAP-N_5 . Future experiments will explore higher photoexcitation energies and further probe the challenging electrochemical reduction of pentazoles.

EXPERIMENTAL SECTION

DMAP-N_5 was synthesized by adaptation of the *Ugi* procedure³² followed by low temperature recrystallization. DMAP-N_3 was obtained by thermolysis of DMAP-N_5 and purified by sublimation. Preparative and analytical details for both compounds can be found in the SI. The ps-TRIR experiments were performed at the Central Laser Facility (CLF) of the Rutherford Appleton Laboratory using the

ULTRA laser and detection system, which was described elsewhere.⁵⁹ The excitation pulses at 310 or 330 nm were generated by an optical parametric amplifier and frequency up-conversion and the IR probe by difference frequency generation of the signal and idler of an optical parametric amplifier. The instrument response of the TRIR system was ca. 200 fs. TRIR spectra were obtained in pump–probe configuration by measuring at 10 kHz the changes in probe IR absorption induced by the pump beam chopped to 5 kHz repetition rate. Background signals due to intensity variations in the IR beam are reduced by subtracting the equivalent signals for the reference (ref) detector. The TRIR transmission spectra are then calculated by $\Delta T = \text{average}[(\text{probe}_{\text{pump on}} - \text{probe}_{\text{pump off}})/\text{probe}_{\text{pump off}}] - \text{average}[(\text{ref}_{\text{pump on}} - \text{ref}_{\text{pump off}})]/\text{average}[\text{ref}_{\text{pump off}}]$. Spectra are converted to change in absorbance (ΔA).⁵⁹ The spectral bandwidth of the IR probe beam is around 400 cm^{-1} and the spectra in the 1200 – 1700 cm^{-1} range were acquired using two spectrometers each with 128 element mercury cadmium telluride detectors (IR Associates) that simultaneously measure two overlapping spectra which are later “stitched” together. Only one spectrometer was required to measure TRIR spectra in the 2000 cm^{-1} region. The spectral resolution was limited by pixel size with a dispersion of $\sim 2 \text{ cm}^{-1}$ per pixel. Probe beam and pump beam had diameters of ~ 100 and $\sim 150 \mu\text{m}$, respectively, in the sample. The capabilities of ULTRA were extended to continuous exchange of the irradiated solution at low temperatures by using a purpose-built, flow apparatus in which solenoid valves, admitting or releasing pneumatic pressure (N_2 , <0.3 bar), control a forward/backward flow of analyte solution between two reservoirs, immersed in a cold bath, via a thermostatized low-temperature spectroscopic cell ($d = 0.1 \text{ mm}$) equipped with CaF_2 windows. Thermally insulated Teflon pipework and heat exchange coils provided the reservoir–cell–reservoir connections and additional cooling. The valve operation was synchronized via a computer program extension to the ULTRA data acquisition software. The sample compartment was purged with N_2 . A thermocouple in direct contact with the solution in the spectroscopic cell recorded the sample temperature. The apparatus can operate at constant sample temperatures ranging from 223 K to ambient. At 233 K, pentazole solutions remained undecomposed for many hours. Further experimental details are given in the SI. Spectral analyses were assisted by spectral line fitting of regions of interest using pseudo Voigt profiles of the type $y = y_0 + A(\mu(2/\pi)(w_L/(4z + w_L^2)) + (1 - \mu)((2(\ln(2))^{1/2}/(\pi^{1/2}w_G))\exp(-(4\ln(2)/w_G^2)z))$, $z = (x - x_c)^2$. Cyclic voltammograms were recorded with an airtight single compartment cell housing Pt microdisc working, Pt coil auxiliary and Ag coil pseudoreference electrodes. $[\text{CoCp}_2]\text{PF}_6$ (Aldrich) served as an internal standard⁶⁰ for the determination of electrode potentials and kinetics of electron transfer. The electrolyte was 0.3 M TBAH (Aldrich, recrystallized twice from absolute EtOH and dried under vacuum at 353 K prior to use) in CH_2Cl_2 distilled from CaH_2 under an atmosphere of dry N_2 . All operations were performed using standard inert gas and vacuum techniques under an overpressure of dry argon. Potential control was maintained with an EG&G PAR model 283 potentiostat. Variable temperature IR spectroelectrochemistry was conducted with an optically transparent thin-layer electrochemical (OTTLE) cell⁶¹ connected to a PA4 potentiostat (Laboratory Devices, Polná, Czech Republic). The IR spectra were recorded at a resolution of 1 cm^{-1} with a Bruker Vertex 70v spectrometer

linked to a Bio-Rad MCT detector unit housing the OTTLE cell in the sample compartment. Filling the OTTLE cell at low temperatures was achieved by differential pressure cannula transfer.

All calculations were performed using Gaussian 09, version C.01⁶² (compiled using Portland compiler v. 8.0–2 with the Gaussian-supplied versions of ATLAS and BLAS^{63,64}) and the B3LYP functional of DFT.⁶⁵ In all cases, an extensive basis set was used, consisting of 6-31G**^{66,67} on all elements. In order to allow for the polarizing effect of the bulk solvent of the experiments, the polarizable continuum model PCM^{68,69} was applied using the standard Gaussian parameters for CH₂Cl₂. The reoptimized geometries using PCM resulted in small changes of bond lengths and angles. Upon convergence, frequencies within the harmonic approximation were calculated and used for comparisons with the recorded IR spectra. All minimum geometries have been identified by the absence of imaginary frequencies, while transition states are characterized by one such frequency. For all converged structures the UV/vis spectrum was calculated using TDDFT for 100 states. GaussSum v. 2.2.5 was employed for the initial analysis of results.⁷⁰ Frequencies were scaled by 0.98 for the fingerprint region and by 0.97 for the ν(N₃)_{as} region in order to account for anharmonicity.⁷¹

■ ASSOCIATED CONTENT

S Supporting Information

Details of the low temperature flow system and settings of the ULTRA ps-TRIR; preparation, purification and infrared (mull, CH₂Cl₂), low temperature UV/vis absorption (CH₃CN), Raman (solid), ¹H and ¹³C NMR spectra (CDCl₃) of DMAP-N₅ and DMAP-N₃; dipoles, total energies, Cartesian coordinates and relative energies concerning the DFT calculations of *N,N*-dimethyl-4-(pentazol-1-yl)aniline (S₀, S₁, and T₁) and cation, 4-azido-*N,N*-dimethylaniline (S₀ and T₁) and cation, 4-λ¹-azanyl-*N,N*-dimethylaniline + N₂ (S₁), 4-λ¹-azanyl-*N,N*-dimethylaniline (S₁ and T₀), and *N,N*-dimethyl-4-azepinamine (S₀) can be found in the SI. This material is available free of charge via the Internet at <http://pubs.acs.org>.

■ AUTHOR INFORMATION

Corresponding Authors

*E-mail: p.portius@sheffield.ac.uk.
*E-mail: f.hartl@reading.ac.uk.

Notes

The authors declare no competing financial interest.

■ ACKNOWLEDGMENTS

The authors acknowledge the support of the STFC council through the programmatic access to the ULTRA facility under the proposal “Real-time Structural Dynamics of Molecular Systems for Energy Generation and Storage” (P.P., Julia Weinstein, and M.T.), and the EPSRC for an advanced research fellowship (PP, E054978/1). I. P. Clark, B. Coles, G. Greetham, and I. Sazanovich are thanked for their assistance in the construction of the low-temperature flow system and the performance of experiments. F.H. thanks the University of Reading for a start-up grant and support of the spectroelectrochemistry laboratory.

■ REFERENCES

- Steinbauer, G.; Klapötke, T. M. “Green” Pyrotechnics: A Chemists’ Challenge. *Angew. Chem., Int. Ed.* **2008**, *47*, 2–20.
- Portius, P.; Fowler, P. W.; Adams, H.; Todorova, T. Z. Experimental and Theoretical Characterization of the Hexaazidophosphate(V) Ion. *Inorg. Chem.* **2008**, *47*, 12004–12009.
- Müller, J. Azides of the Heavier Group 13 Elements. *Coord. Chem. Rev.* **2002**, *235*, 105–119.
- Portius, P.; Davis, M. Recent Developments in the Chemistry of Covalent Main-group Azides. *Coord. Chem. Rev.* **2013**, *257*, 1011–1025.
- Banert, K.; Joo, Y.-H.; Rüffer, T.; Walforth, B.; Lang, H. The Exciting Chemistry of Tetraazidomethane. *Angew. Chem., Int. Ed.* **2007**, *46*, 1168–1171.
- Singh, R. P.; Verma, R. D.; Meshri, D. T.; Shreeve, J. M. Energetic Nitrogen-Rich Salts and Ionic Liquids. *Angew. Chem., Int. Ed.* **2006**, *45*, 3584–3601.
- Stierstorfer, J.; Tarantik, K. R.; Klapötke, T. M. New Energetic Materials: Functionalized 1-Ethyl-5-aminotetrazoles and 1-Ethyl-5-nitriminetetrazoles. *Chem.—Eur. J.* **2009**, *15*, 5775–5792.
- Tang, Y.; Yang, H.; Wu, B.; Ju, X.; Lu, C.; Cheng, G. Synthesis and Characterization of a Stable, Catenated N₁₁ Energetic Salt. *Angew. Chem., Int. Ed.* **2013**, *52*, 4875–4877.
- Köhler, J.; Meyer, R. *Explosives*, 4th ed.; Wiley-VCH: Weinheim, Germany, 1993.
- Tornieporth-Oetting, I. C.; Klapötke, T. M. Covalent Inorganic Azides. *Angew. Chem., Int. Ed. Engl.* **1995**, *34*, 511–520.
- Huynh, M. H. V.; Coburn, M. D.; Meyer, T. J.; Wetzler, M. Green Primary Explosives: 5-Nitrotetrazolato-N₂-ferrate Hierarchies. *Proc. Natl. Acad. Sci. U.S.A.* **2006**, *103*, 10322–10327.
- Haiges, R.; Schneider, S.; Schroer, T.; Christe, K. O. High-Energy-Density Materials: Synthesis and Characterization of N₅[−][P-(N₃)₆][−], N₅⁺[B(N₃)₄][−], N₅^{+[HF₂][−]×nHF}, N₅^{+[BF₄][−], N₅^{+[PF₆][−], and N₅^{+[SO₃F][−]. *Angew. Chem., Int. Ed.* **2004**, *43*, 4919–4924.}}}
- Cacace, F.; de Petris, G.; Troiani, A. Experimental Detection of Tetranitrogen. *Science* **2002**, *295*, 480–481.
- Cacace, F. From N₂ and O₂ to N₄ and O₄: Pneumatic Chemistry in the 21st Century. *Chem.—Eur. J.* **2002**, *8*, 3838–3847.
- Butler, R. N.; Hanniffy, J. M.; Stephens, J. C.; Burke, L. A. A Ceric Ammonium Nitrate N-Dearylation of N-p-Anisylazoles Applied to Pyrazole, Triazole, Tetrazole, and Pentazole Rings: Release of Parent Azoles. Generation of Unstable Pentazole, HN₅/N₅[−], in Solution. *J. Org. Chem.* **2008**, *74*, 1354–1364.
- Schroer, T.; Haiges, R.; Schneider, S.; Christe, K. O. The Race for the First Generation of the Pentazolate Anion in Solution is Far From Over. *Chem. Commun.* **2005**, 1607–1609.
- Östmark, H.; Wallin, S.; Brinck, T.; Carlquist, P.; Claridge, R.; Hedlund, E.; Yudina, L. Detection of Pentazolate Anion (*cyclo*-N₅[−]) from Laser Ionization and Decomposition of Solid *p*-Dimethylaminophenylpentazole. *Chem. Phys. Lett.* **2003**, *379*, 539–546.
- Vij, A.; Pavlovich, J. G.; Wilson, W. W.; Vij, V.; Christe, K. O. Experimental Detection of the Pentaazacyclopentadienide (Pentazolate) Anion, *cyclo*-N₅. *Angew. Chem., Int. Ed.* **2002**, *41*, 3051–3054.
- Straka, M.; Pyykko, P. One Metal and Forty Nitrogens. Ab Initio Predictions for Possible New High-Energy Pentazolides. *Inorg. Chem.* **2003**, *42*, 8241–8249.
- Burke, L. A.; Fazen, P. J. Consideration of Spin States in Determining the Structure and Decomposition of the Transition Metal Pentazoles FeClN₅, Fe(N₅)₂, Fe(H₂O)₄ClN₅, and Fe(NH₃)₄ClN₅. *Chem. Commun.* **2004**, 1082–1083.
- Kobrs, I.; Zheng, W.; Knox, J. E.; Heeg, M. J.; Schlegel, H. B.; Winter, C. H. Experimental and Theoretical Study of the Coordination of 1,2,4-Triazolato, Tetrazolato, and Pentazolato Ligands to the [K(18-crown-6)]⁺ Fragment. *Inorg. Chem.* **2006**, *45*, 8700–8710.
- Frunzke, J.; Lein, M.; Frenking, G. Structures, Metal-Ligand Bond Strength, and Bonding Analysis of Ferrocene Derivatives with Group 15 Heteroligands Fe(η^5 -E₅)₂ and FeCp(η^5 -E₅) (E = N, P, As, Sb). A Theoretical Study. *Organometallics* **2002**, *21*, 3351–3359.

- (23) Tsimpis, A. C.; Chaviara, A. T. Structure, Energetics, and Bonding of First Row Transition Metal Pentazolate Complexes: A DFT study. *Inorg. Chem.* **2004**, *43*, 1273–1286.
- (24) Cheng, L. P.; Li, S.; Li, Q. S. Polynitrogen Clusters Containing Five-Membered Rings. *Int. J. Quantum Chem.* **2004**, *97*, 933–943.
- (25) Belau, L.; Haas, Y.; Zilberg, S. Formation of the cyclo-Pentazolate N_5^- Anion by High-Energy Dissociation of Phenyl-pentazole Anions. *J. Phys. Chem. A* **2004**, *108*, 11715–11720.
- (26) Ugi, I. Five-Membered Rings with Two or More Nitrogen Atoms, Pentazoles. *Compr. Heterocycl. Chem.* **1984**, *5*, 839–845.
- (27) Biesemeier, F.; Müller, U.; Massa, W. Die Kristalstruktur von Phenylpentazol, $\text{C}_6\text{H}_5\text{N}_5$. *Z. Anorg. Allg. Chem.* **2002**, *628*, 1933–1934.
- (28) Wallis, J. D.; Dunitz, J. D. An All-Nitrogen Aromatic Ring System: Structural Study of 4-Dimethylaminophenylpentazole. *J. Chem. Soc. Chem. Comm.* **1983**, 910–911.
- (29) Benin, V.; Kaszynski, P.; Radziszewski, J. G. Arylpentazoles revisited: Experimental and Theoretical Studies of 4-Hydroxyphenyl-pentazole and 4-Oxophenylpentazole Anion. *J. Org. Chem.* **2002**, *67*, 1354–1358.
- (30) Biesemeier, F.; Harms, K.; Müller, U. Pentazole Derivates and Azides Formed from them: Potassium-Crown-Ether Salts of $[\text{O}_3\text{S}-p\text{-C}_6\text{H}_4-\text{N}_5]^-$ and $[\text{O}_3\text{S}-p\text{-C}_6\text{H}_4-\text{N}_3]^-$. *Z. Anorg. Allg. Chem.* **2004**, *630*, 787–793.
- (31) Müller, R.; Wallis, J. D.; von Philipsborn, W. Nitrogen-15 NMR spectroscopy. 14. Direct Proof of Structure for the Pentazole Ring System in Solution by Nitrogen-15 NMR Spectroscopy. *Angew. Chem., Int. Ed. Engl.* **1985**, *97*, 515–517.
- (32) Ugi, I.; Perlinger, H.; Behringer, L. Pentazole. 3. Kristallisierte Aryl-Pentazole. *Chem. Ber.* **1958**, *91*, 2324–2329.
- (33) Ugi, I.; Huisgen, R. Pentazole. 2. Die Zerfallsgeschwindigkeit der Aryl-Pentazole. *Chem. Ber.* **1958**, *91*, 531–537.
- (34) Butler, R. N.; Collier, S.; Fleming, A. F. M. Pentazoles: Proton and Carbon-13 NMR Spectra of Some 1-Arylpentazoles: Kinetics and Mechanism of Degradation of the Arylpentazole System. *J. Chem. Soc., Perkin Trans.* **1996**, 801–803.
- (35) Carlqvist, P.; Östmark, H.; Brinck, T. The Stability of Arylpentazoles. *J. Phys. Chem. A* **2004**, *108*, 7463–7467.
- (36) Bräse, S.; Banert, K., Eds.; *Organic Azides*; John Wiley & Sons, Ltd.: Chichester, U.K., 2010; pp 311–364.
- (37) Gritsan, N. P.; Platz, M. S. Kinetics, Spectroscopy, and Computational Chemistry of Arylnitrenes. *Chem. Rev.* **2006**, *106*, 3844–3867.
- (38) Burdzinski, G. T.; Middleton, C. T.; Gustafson, T. L.; Platz, M. S. Solution Phase Isomerization of vibrationally Excited Singlet Nitrenes to vibrationally Excited 1,2-Dihydroazepine. *J. Am. Chem. Soc.* **2006**, *128*, 14804–14805.
- (39) Tsunoda, T.; Yamaoka, T.; Ikari, K. Photosensitivity of Aromatic Azide Compounds. I. Photosensitivity of Monosubstituted Phenyl Azides. *Kogyo Kagaku Zasshi* **1969**, *72*, 156–162.
- (40) Katritzky, A. R.; Keogh, H. J.; Ohlenrott, S.; Topsom, R. D. Infrared Intensities as a Quantitative Measure of Intramolecular Interactions. XIV. Groups with Donor-Acceptor Character. *J. Am. Chem. Soc.* **1970**, *92*, 6855–6860.
- (41) Hall, J. H.; Fargher, J. M.; Gisler, M. R. Substituent Effects on Spin Delocalization in Triplet Phenylnitrenes. 1. Para-Substituted Phenylnitrenes. *J. Am. Chem. Soc.* **1978**, *100*, 2029–2034.
- (42) Kobayashi, T.; Ohtani, H.; Suzuki, K.; Yamaoka, T. Picosecond and Nanosecond Laser Photolyses of *p*-(Dimethylamino)phenyl Azide in Solution. *J. Phys. Chem.* **1985**, *89*, 776–779.
- (43) Li, Y.-Z.; Kirby, J. P.; George, M. W.; Poliakoff, M.; Schuster, G. B. 1,2-Dihydroazepines from the Photolysis of Substituted Aryl Azides: Analysis of Their Chemical and Physical Properties by Time-Resolved Spectroscopic Methods. *J. Am. Chem. Soc.* **1988**, *110*, 8092–8098.
- (44) Johnson, W. T. G.; Sullivan, M. B.; Cramer, C. J. Meta and Para Substitution Effects on the Electronic State Energies and Ring-Expansion Reactivities of Phenylnitrenes. *Int. J. Quantum Chem.* **2001**, *85*, 492–508.
- (45) Wallin, S.; Östmark, H.; Brinck, T.; Norrefeldt, M.; Rehn, S. *Novel High Energetic Materials: Calculations and Synthesis Attempts of Metal Pentazolates by Electrochemistry*; Swedish Defence Research Agency: Tumba, Sweden, 2006.
- (46) Jacob, G.; Renouard, J. *New Progress in Pentazolate Chemistry*; 44th International Annual Conference of Fraunhofer ICT, Energetic Materials, Karlsruhe, 2012.
- (47) Sheinker, Y. N.; Senyavina, L. B.; Zheltova, V. N. Position and Intensity of the Absorption Band Due to Antisymmetric Valence Vibration of the N_3 Group in the Infrared Spectra of Organic Azides. *Dokl. Akad. Nauk SSSR* **1965**, *160*, 1339–1342.
- (48) Leseticky, L.; Barth, R. N. I.; Sticha, M. T. I. Synthesis and Spectra of N-15 Labeled Phenyl Azides. *Czech. J. Phys.* **2003**, *53*, A777–A782.
- (49) Bhaskar, K. R. Anomalous Band Splittings in the Infrared Spectra of Organic Azides, Dixanthogens, and Isothiocyanates. *Indian J. Chem.* **1967**, *5*, 416–418.
- (50) Dyall, L. K.; Kemp, J. E. The Infrared Spectra of Aryl Azides. *Aust. J. Chem.* **1967**, *20*, 1395–1402.
- (51) Johnson, B. G.; Gill, P. M. W.; Pople, J. A. The Performance of a Family of Density Functional Methods. *J. Chem. Phys.* **1993**, *98*, 5612–5625.
- (52) Andersson, M. P.; Uvdal, P. New Scale Factors for Harmonic Vibrational Frequencies Using the B3LYP Density Functional Method with the Triple-zeta Basis Set 6-311+G(d,p). *J. Phys. Chem. A* **2005**, *109*, 2937–2941.
- (53) Kwok, W.-M.; George, M. W.; Grills, D. C.; Ma, C.; Matousek, P.; Parker, A. W.; Phillips, D.; Toner, W. T.; Towrie, M. Direct Observation of a Hydrogen-Bonded Charge-Transfer State of 4-Dimethylaminobenzonitrile in Methanol by Time-Resolved IR Spectroscopy. *Angew. Chem., Int. Ed.* **2003**, *42*, 1826–1830.
- (54) Levine, B. G.; Martinez, T. J. Isomerization Through Conical Intersections. *Annu. Rev. Phys. Chem.* **2007**, *58*, 613–634.
- (55) Robb, M. A. *Adv. Ser. Phys. Chem.* **2011**, *17*, 3–50.
- (56) Araujo, M.; Lasorne, B.; Bearpark, M. J.; Robb, M. A. The Photochemistry of Formaldehyde: Internal Conversion and Molecular Dissociation in a Single Step? *J. Phys. Chem. A* **2008**, *112*, 7489–7491.
- (57) Falvey, D. E.; Gudmundsdottir, A. D., Eds.; *Intermediates in Chemistry and Biology*; Wiley, New York, 2013; p 6.
- (58) Shields, C. J.; Chrisope, D. R.; Schuster, G. B.; Dixon, A. J.; Poliakoff, M.; Turner, J. J. Photochemistry of Aryl Azides: Detection and Characterization of a Dehydroazepine by Time-Resolved Infrared Spectroscopy and Flash Photolysis at Room Temperature. *J. Am. Chem. Soc.* **1987**, *109*, 4723–4726.
- (59) Greetham, G.; et al. ULTRA: A Unique Instrument for Time-Resolved Spectroscopy. *Appl. Spectrosc.* **2010**, *64*, 1311–1319.
- (60) Stojanovic, R. S.; Bond, A. M. Examination of Conditions under which the Reduction of the Cobaltocenium Cation can be Used as a Standard Voltammetric Reference Process in Organic and Aqueous Solvents. *Anal. Chem.* **1993**, *65*, 56–64.
- (61) Mahabiersing, T.; Luyten, H.; Nieuwendam, R. C.; Hartl, F. Synthesis, Spectroscopy and Spectroelectrochemistry of Chlorocarbonyl{1,2-bis[(2,6-diisopropylphenyl)imino]-acenaphthene- κ 2-N,N'}rhodium(I). *Collect. Czech. Chem. Commun.* **2003**, *68*, 1687–1709.
- (62) Frisch, M. J.; et al. *Gaussian 09*, revision A.2; Gaussian, Inc.: Wallingford, CT, 2009. Full author list is shown in the Supporting Information.
- (63) Whaley, R. C.; Petit, A. Minimizing Development and Maintenance Costs in Supporting Persistently Optimized BLAS. *Software: Pract. Exper.* **2005**, *35*, 101–121.
- (64) Whaley, R. C.; Petit, A.; Dongarra, J. J. Automated Empirical Optimization of Software and the ATLAS project. *Parallel Comput.* **2001**, *27*, 3–35.
- (65) Becke, A. D. Density-Functional Thermochemistry. III. The Role of Exact Exchange. *J. Chem. Phys.* **1993**, *98*, 5648–5652.
- (66) McLean, A. D.; Chandler, G. S. Contracted Gaussian Basis Sets for Molecular Calculations. I. Second Row Atoms, $Z = 11 - 18$. *J. Chem. Phys.* **1980**, *72*, 5639–5648.

- (67) Krishnan, R.; Binkley, J. S.; Seeger, R.; Pople, J. A. Self-Consistent Molecular Orbital Methods. XX. A Basis Set for Correlated Wave Functions. *J. Chem. Phys.* **1980**, *72*, 650–654.
- (68) Mennucci, B.; Tomasi, J. Continuum Solvation Models: A New Approach to the Problem of Solute's Charge Distribution and Cavity Boundaries. *J. Chem. Phys.* **1997**, *106*, 5151–5158.
- (69) Cossi, M.; Barone, V.; Mennucci, B.; Tomassi, J. Ab Initio Study of Ionic Solutions by a Polarizable Continuum Dielectric Model. *Chem. Phys. Lett.* **1998**, *286*, 253–286 and references therein.
- (70) O'Boyle, N. M.; Tenderholt, A. L.; Langner, K. M. Software News and Updates cclib: A Library for Package-Independent Computational Chemistry Algorithms. *J. Comput. Chem.* **2008**, *29*, 839–845.
- (71) Irikura, K. K.; Johnson, R. D.; Kacker, R. N. Uncertainties in Scaling Factors for ab Initio Vibrational Frequencies. *J. Phys. Chem. A* **2005**, *109*, 8430–8437.